Inorg. Chem. **2004**, *43*, 1046–1055

X-ray Absorption Spectroscopic Studies of Chromium(V/IV/III)–2-Ethyl-2-hydroxybutanoato(2–/1–) Complexes

Aviva Levina,[†] Rachel Codd,[†] Garry J. Foran,[‡] Trevor W. Hambley,[†] Thomas Maschmeyer,[†] Anthony F. Masters,[†] and Peter A. Lay*[,†]

Centre for Structural Biology and Structural Chemistry and Centre for Heavy Metals Research, School of Chemistry, University of Sydney, Sydney, NSW 2006, Australia, and Australian Nuclear Science and Technology Organisation, PMB 1, Menai, NSW 2234, Australia

Received July 25, 2003

Structures of the complexes $[Cr^{V}O(ehba)_2]^-$, $[Cr^{IV}O(ehbaH)_2]^0$, and $[Cr^{III}(ehbaH)_2(OH_2)_2]^+$ ($ehbaH_2$ = 2-ethyl-2-hydroxybutanoic acid) in frozen aqueous solutions (10 K, [Cr] = 10 mM, 1.0 M $ehbaH_2$/ehbaH, pH 3.5) have been determined by single- and multiple-scattering fitting of X-ray absorption fine structure (XAFS) data. An optimal set of fitting parameters has been determined from the XAFS calculations for a compound with known crystal structure, $Na[Cr^{V}O(ehba)_2]$ (solid, 10 K). The structure of the Cr(V) complex $[Cr^{V}O(ehba)_2]^-$ does not change in solution in the presence of excess ligand. Contrary to the earlier suggestions made from the kinetic data (Ghosh, M. C.; Gould, E. S. *J. Chem. Soc., Chem. Commun.* **1992**, 195–196), the structure of the Cr(IV) complex (generated by the Cr(VI) + As(III) + $ehbaH_2$ reaction) is close to that of the Cr(V) complex (five-coordinate, distorted trigonal bipyramidal) and different from that of the Cr(III) complex (six-coordinate, octahedral). For both Cr(V) and Cr(IV) complexes, some disorder in the position of the oxo group is observed, which is consistent with but not definitive for the presence of geometric isomers. The structure of the Cr(IV) complex differs from that of Cr(V) by protonation of alcoholato groups of the ligands, which leads to significant elongation of the corresponding Cr–O bonds (2.0 vs 1.8 Å). This is reflected in the different chemical properties reported previously for the Cr(IV) and Cr(V) complexes, including their reactivities toward DNA and other biomolecules in relation to Cr-induced carcinogenicity.

Introduction

Recent interest in the aqueous solution chemistry of Cr(V/IV)[1−5] is primarily due to the proposed roles of these highly reactive oxidation states as DNA-damaging species in Cr(VI)-induced mutagenesis and carcinogenesis.[6,7] Relatively stable Cr(V/IV)−ehba[8] complexes are extensively used as models for understanding the Cr(V/IV) reactions with biomolecules.[4,5,7,9−14] These complexes are likely to mimic the Cr(V/IV) complexes of biological 2-hydroxycarboxylates, such as citrate or lactate, that could be formed during the intracellular reduction of Cr(VI).[15] Studies of redox reactions of well-characterized Cr(V/IV) complexes are also important

* Author to whom correspondence should be addressed. E-mail: p.lay@chem.usyd.edu.au.

[†] University of Sydney.

[‡] Australian Nuclear Science and Technology Organisation.

(1) Farrell, R. P.; Lay, P. A. *Comments Inorg. Chem.* **1992**, *13*, 133−175 and references therein.
(2) Barr-David, G.; Charara, M.; Codd, R.; Farrell, R. P.; Irwin, J. A.; Lay, P. A. Bramley, R.; Brumby, S.; Ji, J.-Y.; Hanson, G. R. *J. Chem. Soc., Faraday Trans.* **1995**, *91*, 1207−1216 and references therein.
(3) Gould, E. S. *Coord. Chem. Rev.* **1994**, *135/136*, 651−684 and references therein.
(4) Codd, R.; Dillon, C. T.; Levina, A.; Lay, P. A. *Coord. Chem. Rev.* **2001**, *216−217*, 533−577.
(5) Levina, A.; Codd, R.; Dillon, C. T.; Lay, P. A. *Prog. Inorg. Chem.* **2003**, *51*, 145−250.
(6) Connett, P.; Wetterhahn, K. E. *Struct. Bonding (Berlin)* **1983**, *54*, 93−124.
(7) Levina, A.; Barr-David, G.; Codd, R.; Lay, P. A.; Dixon, N. E.; Hammershøi, A.; Hendry, P. *Chem. Res. Toxicol.* **1999**, *12*, 371−381 and references therein.
(8) Abbreviations: $ehbaH_2$ = 2-ethyl-2-hydroxybutanoic acid; FT = Fourier transform; MM = molecular mechanics; MS = multiple scattering; SS = single scattering; XAFS = X-ray absorption fine structure; XANES = X-ray absorption near-edge structure; XAS = X-ray absorption spectroscopy.
(9) Sugden, K. D.; Wetterhahn, K. E. *J. Am. Chem. Soc.* **1996**, *118*, 10811−10818.
(10) Sugden, K. D.; Wetterhahn, K. E. *Chem. Res. Toxicol.* **1997**, *10*, 1397−1406.
(11) Bose, R. N.; Fonkeng, B. S.; Moghaddas, S.; Stroup, D. *Nucleic Acids Res.* **1998**, *26*, 1588−1596.
(12) Lay, P. A.; Levina, A. *J. Am. Chem. Soc.* **1998**, *120*, 6704−6714.
(13) Levina, A.; Lay, P. A.; Dixon, N. E. *Inorg. Chem.* **2000**, *39*, 385−395.
(14) Levina, A.; Bailey, A. M.; Champion, G.; Lay, P. A. *J. Am. Chem. Soc.* **2000**, *122*, 6208−6216.
(15) Codd, R.; Lay, P. A. *J. Am. Chem. Soc.* **1999**, *121*, 7864−7876.

10.1021/ic030239r CCC: $27.50
Published on Web 01/07/2004

Table 1. XAS Experimental Settings

parameter	SSRL (solutions)	ANBF (solutions)	ANBF (solids)
beam energy, GeV	3.0	2.5	
beam current, mA	50−100	250−400	
light source	wiggler (eight periods)	bending magnet	
beamline	9-3 (focused)	20B (unfocused)	
monochromator crystal	double crystal Si[220], nondetuned	channel-cut Si[111], detuned by 50%	
detection method	fluorescence		transmission
detector	30-element Ge array (Canberra)	10-element Ge array (Canberra)	N_2/He (1:1)-filled ionization chambers
energy calibration	Cr foil, first inflection point of the edge assigned to 5989.0 eV		
scan range and step size (in parentheses), eV	5770−5970 (10), 5970−6050 (0.25), 6050−7000 (2−6, 0.05 Å^{-1} in *k*-space)		
sample thermostating	continuous flow liquid He, 10 ± 1 K	closed cycle He gas (CryoIndustries), 10 ± 1 or 293 K	
sample form	solution in H_2O, ∼0.05% (mass) Cr		mixture with BN, ∼10% (mass) Cr
sample cell	lucite (23 × 3 × 2 mm), Mylar tape windows	polycarbonate (10 × 10 × 2 mm), Kapton windows	Al (10 × 10 × 0.5 mm), Kapton windows
no. of scans	2 scans at each of 6 spots	2 scans at each of 5 spots	1 scan at each of 2 spots
av scan time, min	30	40	

for understanding general mechanisms of electron transfer in coordination compounds.[16]

The Cr(V) complex $Na[Cr^{V}O(ehba)_2]$ has been isolated from the reaction of Cr(VI) with $ehbaH_2$ in acetone,[17] and its crystal structure has been determined.[18] By contrast, the Cr(IV)−ehba complex, which can be generated quantitatively by the Cr(VI) + As(III) + $ehbaH_2$ reaction in aqueous solutions (pH 2−4),[19] is too unstable to be crystallized.[20,21] Alternative structures of this complex, $[Cr^{IV}(ehbaH)_2(OH)_2]^0$ (six-coordinate, octahedral) or $[Cr^{IV}O(ehbaH)_2]^0$ (five-coordinate, distorted trigonal bipyramidal), have been suggested from UV−vis spectroscopic and electrochemical studies.[19−23] Direct determination of the Cr coordination environment by XAS[24,25] is required to distinguish between these possibilities.

Recently, a preliminary account of the first XAS study of Cr(V/IV/III)−ehba complexes in frozen aqueous solutions was reported, which led to determination of the first solution structure of a Cr(IV) complex, $[Cr^{IV}O(ehbaH)_2]^0$.[26] In the current work, a detailed comparative XAS study of ehba complexes of the three oxidation states of Cr has been performed, using data of much higher quality compared with those used in the preliminary work.[26] In addition, advantages and limitations of XAS in the determination of three-dimensional structures of such metal complexes have been examined for the crystallographically characterized compound $Na[Cr^{V}O(ehba)_2]$.[17,18]

Experimental Section

Caution. *Cr(VI) and As(III) compounds are human carcinogens,[27,28] and Cr(V/IV) complexes are mutagenic and potentially carcinogenic.[29] Contact with skin and inhalation must be avoided.*

Reagents. The following commercial reagents of analytical or higher purity grade were used without purification: 2-ethyl-2-hydroxybutanoic acid, acetone, BN, As_2O_3, $Na_2CrO_4 \cdot 4H_2O$, CrO_2, and NaOH (all from Aldrich) and $FeSO_4 \cdot 7H_2O$ (Merck). Synthesis of $Na[Cr^{V}O(ehba)_2] \cdot H_2O$ was performed by a literature method,[17] and its purity was confirmed by IR, UV−vis, and EPR spectroscopies.[17,18]

Sample Preparation and Data Collection. Solutions of Cr(IV) were generated by the reaction of Cr(VI) (10 mM) with As(III) (0.10 M) and $ehbaH_2$/ehbaH (1.0 M, pH 3.5) at ∼4 °C.[19,21] The reaction mixture was injected into the XAS cell and frozen in liquid N_2 within 50 s after mixing of the reagents. At the time of freezing, the yield of Cr(IV) was ≥92% $[Cr(VI)]_0$ (determined by UV−vis spectroscopy,[21] using an HP 8452A diode-array spectrophotometer). A solution of Cr(V) was prepared by dissolving $Na[Cr^{V}O(ehba)_2]$ (10 mM) in $ehbaH_2$/ehbaH (1.0 M, pH 3.5). The reaction of $Na[Cr^{V}O(ehba)_2]$ (10 mM) with $FeSO_4$ (50 mM) in $ehbaH_2$/ehbaH (1.0 M, pH 3.5, reaction time ∼1 min at 20 °C) led to the formation of a Cr(III)−ehba complex (proposed structure $[Cr^{III}(ehbaH)_2(OH_2)_2]^+$).[30] The solutions of Cr(V) and Cr(III) were stable for at least 15 min at 20 °C (UV−vis spectroscopy) and were frozen in liquid N_2 ∼2 min after the preparation. Solid samples of $Na[Cr^{V}O(ehba)_2]$ or CrO_2 were mixed with BN to obtain ∼10% (by weight) Cr. Chromium K-edge spectra were recorded on beamline 9-3 at the Stanford Synchrotron Radiation Laboratory (SSRL) or at the Australian National Beamline Facility (ANBF, beamline 20B) at the Photon Factory (Tsukuba, Japan). Experimental settings are

(16) (a) Bakac, A. *J. Am. Chem. Soc.* **2000**, *122*, 1092−1097. (b) Bakac, A.; Guzei, I. A. *Inorg. Chem.* **2000**, *39*, 736−740.
(17) Krumpolc, M.; Roček, J. *J. Am. Chem. Soc.* **1979**, *101*, 3206−3209.
(18) Judd, R. J.; Hambley, T. W.; Lay, P. A. *J. Chem. Soc., Dalton Trans.* **1989**, 2205−2210.
(19) Ghosh, M. C.; Gould, E. S. *Inorg. Chem.* **1991**, *30*, 491−494.
(20) Ghosh, M. C.; Gelerinter, E.; Gould, E. S. *Inorg. Chem.* **1992**, *31*, 702−705.
(21) Codd, R.; Lay, P. A.; Levina, A. *Inorg. Chem.* **1997**, *36*, 5440−5448.
(22) (a) Ghosh, M. C.; Gould, E. S. *J. Chem. Soc., Chem. Commun.* **1992**, 195−196. (b) Ghosh, M. C.; Gould, E. S. *J. Am. Chem. Soc.* **1993**, *115*, 3167−3173.
(23) Bose, R. N.; Fonkeng, B.; Barr-David, G.; Farrell, R. P.; Judd, R. J.; Lay, P. A.; Sangster, D. F. *J. Am. Chem. Soc.* **1996**, *118*, 7139−7144.
(24) Penner-Hahn, J. E. *Coord. Chem. Rev.* **1999**, *190−192*, 1101−1123.
(25) Codd, R.; Levina, A.; Zhang, L.; Hambley, T. W.; Lay, P. A. *Inorg. Chem.* **2000**, *39*, 990−997.
(26) Levina, A.; Foran, G. J.; Lay, P. A. *J. Chem. Soc., Chem. Commun.* **1999**, 2339−2340.
(27) IARC. *Monographs on the Evaluation of the Carcinogenic Risk of Chemicals to Humans. Vol.49. Chromium, Nickel and Welding*; International Agency on the Research of Cancer: Lyon, France, 1990; see also references therein.
(28) Leonard, A.; Lauwerys, R. R. *Mutat. Res.* **1980**, *75*, 49−62 and references therein.
(29) Dillon, C. T.; Lay, P. A.; Bonin, A. M.; Cholewa, M.; Legge, G. J. F.; Collins, T. J.; Kostka, K. L. *Chem. Res. Toxicol.* **1998**, *11*, 119−129 and references therein.
(30) Bose, R. N.; Gould, E. S. *Inorg. Chem.* **1985**, *24*, 2832−2835.

listed in Table 1. Data collection at low temperature (10 K) minimized photodamage of the samples, improved the signal-to-noise ratio, and maximized the MS contribution to the XAFS spectrum.[31]

XAS Data Processing. Averaging, background subtraction, and the calculations of theoretical XAFS spectra were performed using the XFIT software package,[32] including FEFF 4.06[33] and FEFF 6.01[34] algorithms (for SS and MS, respectively), as described previously.[31] Conditions, restraints, and constraints, applied to the calculations, are listed in Table S1 (Supporting Information). Fourier filtering has been applied in MS XAFS calculations to reduce the noise in the XAFS data at high k values.[32] Variations of the Fourier window parameters did not significantly affect the outcome of the MS XAFS calculations (see the Results). Overdeterminacy of the models used for both SS and MS XAFS calculations was checked by the method of Binsted et al.,[35] taking into account the applied restraints and constraints. In all MS XAFS calculations, the values of bond lengths and bond angles within the ehba ligands were restrained to be close (±0.05 Å, ±5°) to those found in the crystal structure of $Na[Cr^{V}O(ehba)_2]$.[18] Release of these restraints led to underdetermined models and to implausible distortions in the ligand structures. Debye−Waller factors of similar atoms in the ehba ligands were constrained to be equal, to decrease the number of variables in the models. The random errors in the estimated XAFS parameters, arising from the noise in the data, were determined by Monte Carlo analysis within the XFIT software.[32] Starting coordinate sets used for MS XAFS calculations were obtained from the crystal structures of $Na[Cr^{V}O(ehba)_2]$[18] or $NH_4[V^{IV}O(ehba)(ehbaH)]$,[36] from the results of MM calculations for $Na[Cr^{V}O(ehba)_2]$,[37] or from the molecular models generated by HyperChem software (based on electronic states of the atoms, no experimental data involved).[38] The corresponding models are shown in Chart 1.

MM Calculations. The energy-optimized structure of $Na[Cr^{V}O(ehba)_2]$ was determined[37] using MOMEC software.[39] The force field (Table S2 in the Supporting Information) was developed[37] using both published[40,41] force constants and those determined from the IR data.[37] The starting coordinate set was obtained from the crystal structure of $Na[Cr^{V}O(ehba)_2]$.[18] The force field partially constrained the metal-center geometry, which was necessary for modeling the different coordination spheres of the geometrical isomers of Cr(V)−2-hydroxyacid complexes (Table S3 in the Supporting Information).[42] The X-ray crystal structure coordinates of $[Cr^{V}O(ehba)_2]^-$ compared well to the coordinates generated by molecular-mechanics calculations of $[Cr^{V}O(ehba)_2]^-$ (the calculated bond lengths and angles were within 0.02 Å and 2°, respectively, of those determined by X-ray crystallography),[37] which indicates the validity of the force field used in the calculations. The minimization function was based on the Newton−Raphson method,[43] which was applied until the shift in the positional coordinates was less than 0.001 Å.

Chart 1. Models Used for Initiation of MS XAFS Calculations[a]

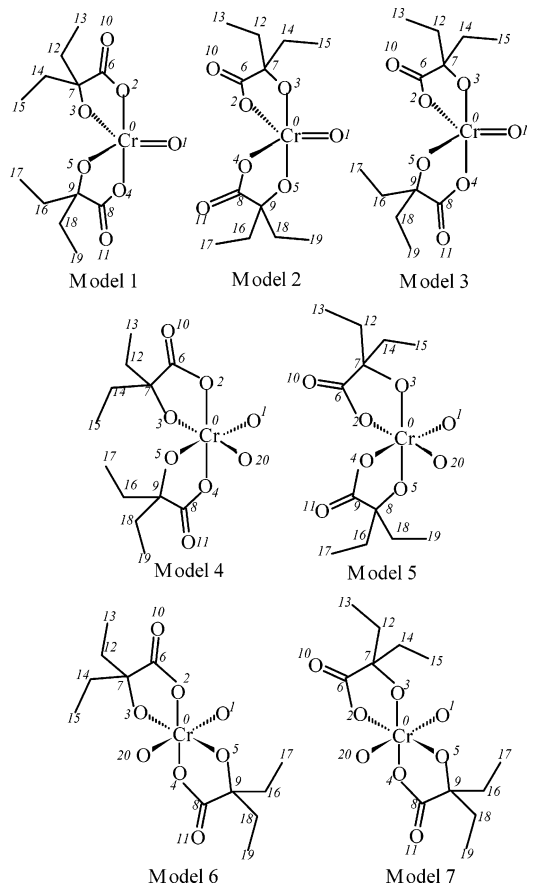

[a] See the text. The atom numbering corresponds to those used in Tables S1 and S5−S10 (Supporting Information).

Results

Stability of Cr(V/IV/III)−ehba Complexes Under the XAS Conditions. During the data collection at the SSRL, some decomposition of the samples was evident from (i) color changes in the irradiated spots of the frozen samples (only for Cr(V); red coloration appeared, which is indicative for Cr(IV)),[19,21] (ii) changes in UV−vis spectra of the irradiated samples after thawing, compared to the initial solutions (Figure 1), and (iii) changes in the XANES spectra for two sequential scans taken at the same spot (Figure S1a−c in the Supporting Information). The degree of photodamage, measured from the changes in the edge energy, decreased in the following order: Cr(V) > Cr(IV) > Cr(III) (Figure S1a−c). The increase in absorbance at 300−800 nm for the Cr(V) sample after irradiation (Figure 1) is consistent with the formation of some Cr(IV) due to photoreduction.[19,21] The decrease in absorbance at 300−600

(31) (a) Rich, A. M.; Armstrong, R. S.; Ellis, P. J.; Freeman, H. C.; Lay, P. A. *Inorg. Chem.* **1998**, *37*, 5743−5753. (b) Rich, A. M.; Armstrong, R. S.; Ellis, P. J.; Lay, P. A. *J. Am. Chem. Soc.* **1998**, *120*, 10827−10836.
(32) (a) Ellis, P. J.; Freeman, H. C. *J. Synchrotron Radiat.* **1995**, *2*, 190−195. (b) *XFIT for Windows'95*; Australian Synchrotron Research Program: Sydney, Australia, 1996.
(33) Mustre de Leon, J.; Rehr, J. J.; Zabinsky, S. I.; Albers, R. C. *Phys. Rev. B* **1991**, *44*, 4146−4156.
(34) Zabinsky, S. I.; Rehr, J. J.; Ankudinov, A.; Albers, R. C.; Eller, M. J. *Phys. Rev. B* **1995**, *52*, 2995−3009.
(35) Binsted, N.; Strange, R. W.; Hasnain, S. S. *Biochemistry* **1992**, *31*, 12117−12125.
(36) Barr-David, G.; Hambley, T. W.; Irwin, J. A.; Judd, R. J.; Lay, P. A.; Martin, B. D.; Bramley, R.; Dixon, N. E.; Hendry, P.; Ji, J.-Y.; Baker, R. S. U.; Bonin, A. M. *Inorg. Chem.* **1992**, *31*, 4906−4908.
(37) Codd, R. B.Sc.(Hons) Thesis, University of Sydney, Sydney, Australia, 1992.
(38) *HyperChem*, Version 5.1; Hypercube Inc.: Gainesville, FL, 1996.
(39) Hambley, T. W. *MOMEC 87. Program for Strain-Energy Minimization*; University of Sydney: Sydney, Australia, 1987.
(40) Hambley, T. W. *Acta Crystallogr., Sect. B* **1988**, *44B*, 601−609.
(41) Auf der Heyde, T. P. E.; Nassimbeni, L. R. *Acta Crystallogr., Sect. B* **1984**, *40B*, 582−590.
(42) Bramley, R.; Ji, J.-Y.; Judd, R. J.; Lay, P. A. *Inorg. Chem.* **1990**, *29*, 3089−3094.
(43) Boyd, R. H. *J. Chem. Phys.* **1968**, *49*, 2574−2583.

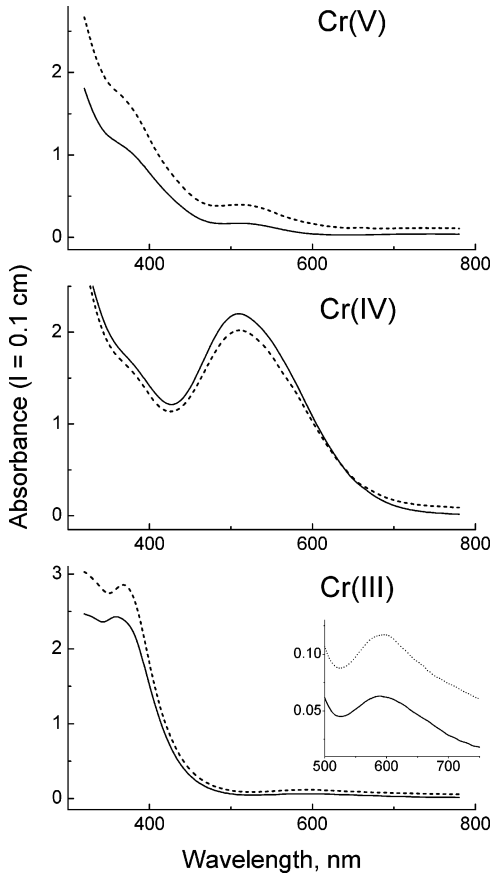

Figure 1. UV−vis spectra of solutions of the Cr(V/IV/III)−ehba complexes (10 mM Cr, 1.0 M ehbaH_2/ehbaH, pH 3.5, ∼20 °C) before (solid lines) and after (dashed lines) the irradiation at the SSRL.

nm and increase in absorbance at 650−800 nm for the Cr(IV) sample (Figure 1) are due to its partial disproportionation with the formation of Cr(V) and Cr(III).[20,21] The increase in absorbance at 300−800 nm for the Cr(III) sample in the presence of excess Fe(II) is probably due to the photochemical reactions of Fe(III/II), as the specific absorbance of Cr(III) at ∼600 nm did not change significantly (Figure 1). To minimize the influence of photodamage on the results of XAFS modeling, only the first scans at each spot were used to obtain the averaged spectra (for the data collected at the SSRL). As reported previously,[25,26] no evidence of photodamage was obtained for the data collected at the ANBF (Figure S1d), and averages of all scans were used for data processing in this case. This was used to validate that the better quality SSRL data were not compromised by photodecomposition. Thus, the use of the brighter and focused beam together with a 30-element detector at the SSRL (Table 1) significantly improves the signal-to-noise ratio in the XAFS spectra of dilute solutions of Cr(V/IV/III) (see below), but increases the photodamage of the samples.

XANES Spectra of Cr(V/IV/III)−ehba Complexes. The pre-edge and edge features for the complexes with different oxidation states of Cr are compared in Figure 2a; the energies are given in Table 2. These energies are the same, within experimental error, as those for the XANES spectra of Cr(V/IV/III)−ehba complexes, collected at the ANBF (where

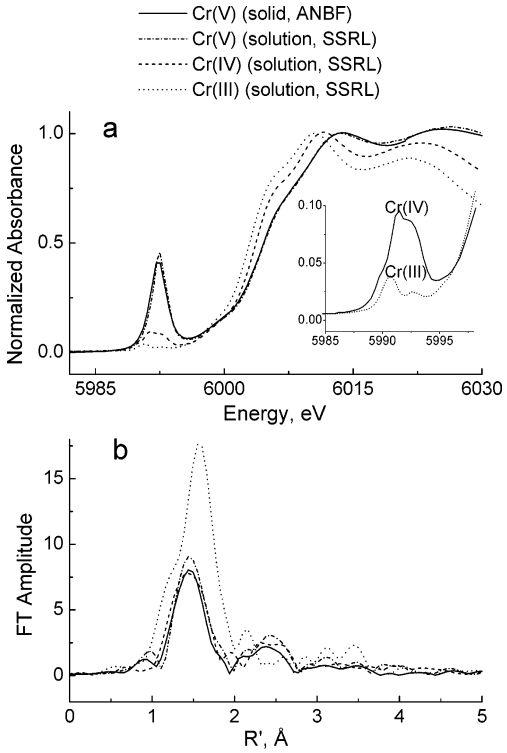

Figure 2. Comparison of XANES spectra (a) or FT XAFS spectra (b) for the Cr(V/IV/III)−ehba complexes.

no significant photodamage of the samples occurred).[26] In agreement with the results of preliminary studies[26] and the literature data for Cr(III) and Cr(V) complexes,[25,44,45] the edge energy and the intensity of pre-edge absorbance decrease in the following order: Cr(V) > Cr(IV) > Cr(III). The XANES spectra for the solid Na[$Cr^{V}O$(ehba)$_2$] and its aqueous solution (10 mM, in the presence of 1.0 M ligand) are practically identical (Figure 2a). Thus, the five-coordinate structure of the Cr(V) complex is retained in solution, even in the presence of a large excess of ligand. The XANES spectral features of Na[$Cr^{V}O$(ehba)$_2$] closely resemble those of another five-coordinate Cr(V)−2-hydroxycarboxylato complex, Na[$Cr^{V}O$(qa)$_2$] (qa = quinato(2−) = 1(*R*),3(*R*),4(*R*),5(*R*)-tetrahydroxycyclohexanecarboxylato(2−).[25] The intensity of the pre-edge absorbance for both complexes was significantly higher than that for a dimeric Cr(V)−alaninato complex, [Cr^{V}_2(μ-O)$_2$(O)$_2$(Ala)$_2$(OMe)$_2$]$^{2-}$, possessing six-coordinate Cr(V) centers.[46] The spectra for solutions of the Cr(IV)−ehba complex, collected at the SSRL or at the ANBF are similar, except for the higher signal-to-noise ratio in the former (Figure S2 in the Supporting Information). The edge energy and the intensity of the pre-edge peak for the Cr(IV) complex are similar to those of the stable Cr(IV) compound CrO_2 (Figure S3 in the Supporting Information). The edge features and the energies of pre-edge absorbance, however, are different, which is indicative of different coordination

(44) Ellis, P. J.; Joyner, R. W.; Maschmeyer, T.; Masters, A. F.; Niles, D. A.; Smith, A. K. *J. Mol. Catal. A* **1996**, *111*, 297−305.
(45) Dillon, C. T.; Lay, P. A.; Cholewa, M.; Legge, G. J. F.; Bonin, A. M.; Collins, T. J.; Kostka, K. L.; Shea-McCarthy, G. *Chem. Res. Toxicol.* **1997**, *10*, 533−535.
(46) Headlam, H. A.; Weeks, C. L.; Turner, P.; Hambley, T. W.; Lay, P. A. *Inorg. Chem.* **2001**, *40*, 5097−5105.

Table 2. Summary of XAS Results

parameter	Cr(V) solid[a] (ANBF)	Cr(V) soln[b] (SSRL)	Cr(IV) soln[b] (SSRL)	Cr(IV) soln[b] (ANBF)	Cr(III) soln[b] (SSRL)
			XANES[c]		
pre-edge, eV	5992.5	5992.5	5991.5, 5992.7	5993	5990.7, 5992.7
edge,[d] eV	6004.5	6004.5	6003.7	6004.0	6003.0
			XAFS[e]		
oxo					
X, Å	1.56 (1.557)[f]	1.57	1.56	1.54	
σ_i^2, Å^2	0.0043	0.0022	0.0063	0.0025	
ROH/RO$^-$					
X, Å	1.80[g] (1.799)[f]	1.80[g]	2.00[h]	2.02[h]	1.98[h]
σ_i^2, Å^2	0.0044	0.0034	0.0010	0.0010	0.0010
RCO$_2^-$					
X, Å	1.89 (1.900)[f]	1.90	1.90	1.91	1.90
σ_i^2, Å^2	0.0015	0.0010	0.0020	0.0010	0.0010
H$_2$O					
X, Å					1.97
σ_i^2, Å^2					0.0010
$-\Delta E_0$, eV	6.7	3.8	2.1	3.8	6.2
S_0^2	0.89	0.90	0.89	0.92	0.92
N_i/p	1.2	1.2	1.1	1.0	1.2
R,[i] %	11	17	12	12.5	17

[a] Identical results (within experimental error) were obtained at 10 or 293 K. [b] Frozen solutions at 10 K. [c] Figure 2a; energy values of two main pre-edge peaks of Cr(IV) and Cr(III) are given. [d] Measured at 50% of the edge jump. [e] Results of MS fits of XAFS spectra; experimental and calculated spectra are shown in Figure 3, and calculation details are given in Tables S1 and S5−S10. The results were independent (within experimental error) of the initial model used (models 1 and 2 for Cr(V) or Cr(IV), models 4−7 for Cr(III), Chart 1). Definitions: X is the Cr−O bond length; σ_i^2 are the Debye−Waller factors; $\Delta E_0 = E_0 - 6005$ eV, where E_0 is the threshold energy; S_0^2 is a scale factor; N_i/p is the determinancy parameter of the calculation (where N_i is the number of independent observations and p is the number of varied parameters);[35] R is the goodness-of-fit parameter. Errors in the optimized values, arising from the noise in the data (estimated by the Monte Carlo method)[32] were <0.005 Å for X, <0.0003 Å^2 for σ_i^2, <0.2 eV for ΔE_0, and <0.01 for S_0^2. Expected systematic errors in the X values are 0.01−0.02 Å.[31] [f] Values from the crystal structure of Na[Cr^{V}O(ehba)$_2$][18] are given in parentheses. [g] Deprotonated. [h] Protonated. [i] Smaller R values correspond to a better fit; fits with R < 20% are considered as good.[35]

geometries.[47] To our knowledge, no other XANES data for Cr(IV) complexes are available for comparison.

SS XAFS Fitting. Representative results of SS XAFS modeling of the first coordination shells in Cr(V/IV/III)−ehba complexes are given in Table S4 (Supporting Information). Acceptable models were those possessing both low goodness-of-fit values (R < 15%) and physically reasonable values of the fitting parameters: the threshold energy E_0, the scale factor S_0^2, and the Debye−Waller factors σ_i^2 (the acceptable ranges of these values are given in Table S1).[32] The models where the numbers of scatterers were included in the variables gave optimal coordination numbers close to 5 for both the Cr(V) and Cr(IV) complexes and close to 6 for the Cr(III) complex (models 1, 2, 9, 10, 17, 18, and 25 in Table S4). The best fit to the XAFS data for the Cr(V) complex in both the solid state and in solution (models 4 and 12 in Table S4) included one short (1.55 Å), two intermediate (1.80 Å), and two long (1.90 Å) Cr−O bonds, corresponding to the oxo, alcoholato (deprotonated), and carboxylato ligands, respectively, in the crystal structure of Na[Cr^{V}O(ehba)$_2$].[18] The best fit for the Cr(IV) complex (model 20 in Table S4) included, in addition to one oxo bond (1.55 Å) and two carboxylato Cr−O bonds (1.88 Å), two longer bonds (1.98 Å) corresponding to Cr binding to the protonated alcoholato group of ebhaH.[36] For both the Cr(V) and Cr(IV) complexes, application of models including six Cr−O bonds, while giving acceptable R values, led to unreasonably high σ_i^2 values (models 5−8, 13−16, and 21−24 in Table S4). For the Cr(III) complex, the best SS XAFS fit (model 26 in Table S4) included six equal Cr−O bonds (1.95 Å); application of models with different Cr−O bonds lengths led to unreasonably low σ_i^2 values (models 27−29 in Table S4). Thus, the differences in Cr−O bond lengths (if any) for the Cr(III) complex are below the resolution limit of SS XAFS fitting (~0.1 Å for the XAFS spectrum with $k_{max} = 16$).[25,31]

The results of SS XAFS modeling (Table S4) suggest that the structures of the first coordination shells in the Cr(V) and Cr(IV) complexes are similar, and differ from that of the Cr(III) complex. This suggestion is supported by comparison of FT XAFS spectra of the Cr(V/IV/III) complexes (Figure 2b). A marked increase in the amplitude of the first FT peak for the Cr(III) complex, compared to those of the Cr(V) and Cr(IV) complexes, indicates an increase in coordination number.[48] In summary, the results of SS XAFS modeling, in agreement with the results of preliminary studies[26] and the literature data,[18,21,30] provided strong evidence that the complexes were [Cr^{V}O(ehba)$_2$]$^-$, [Cr^{IV}O(ehbaH)$_2$]^0, and [Cr^{III}(ehbaH)$_2$(OH$_2$)$_2$]$^+$.

MM Calculations for [Cr^{V}O(ehba)$_2$]$^-$. Experimental evidence for the existence of several geometric isomers of [Cr^{V}O(ehba)$_2$]$^-$ in solutions has been gained from EPR spectroscopy.[42] The postulated isomers (models 1−3 in Chart 1) are variants of a distorted trigonal bipyramid with different arrangements of carboxylato and alcoholato groups around the Cr center.[1] Other isomers are possible, with the oxo group occupying an axial position, but these are likely to be much

(47) Solid CrO_2 possesses a six-coordinate, rutile-type structure (Cotton, F. A.; Wilkinson, G.; Murillo, C. A.; Bochmann, M. *Advanced Inorganic Chemistry*, 6th ed.; John Wiley and Sons: New York, 1999; p 740).

(48) Dooley, D. M.; Scott, R. A.; Knowles, P. F.; Colangelo, C. M.; McGuirl, M. A.; Brown, D. E. *J. Am. Chem. Soc.* **1998**, *120*, 2599−2605.

Table 3. Summary of MM Calculation Results for the Geometric Isomers of $[Cr^{V}O(ehba)_2]^{-}$ [a]

parameter	model 1	model 2	model 3
total strain energy, kJ mol^{-1}	34.8	32.0[c]	36.4
energy contributions, kJ mol^{-1}			
bond-length deformations	4.59	4.61	4.56
valence-angle deformations	9.77	9.74	10.00
torsional deformations	0.59	0.41	0.69
nonbonded interactions	19.80	17.25	21.18
out-of-plane deformations	0.00	0.00	0.00
interligand plane angle,[b] deg	140.1[d]	128.0[c]	151.3

[a] Designations of the models correspond to Chart 1. Force field parameters, applied in the calculations, are listed in Tables S2 and S3, Supporting Information. [b] The angle between the plane defined by atoms Cr0, O2, C6, C7, O3, and O10 and the plane defined by atoms Cr0, O4, O5, C8, C9, and O11 (Chart 1). [c] The values of total strain energy and interligand plane angle for the optimized MM model of $[Cr^{V}O(ehba)_2]^{-}$ (without geometry constraints around the Cr atom) were 31.5 kJ mol^{-1} and 125.2°, respectively. [d] The corresponding value in the crystal structure of $Na[Cr^{V}O(ehba)_2]$ was 134.9°.[18]

less stable.[37] The values of relative strain energies for the three postulated isomers, calculated by the MM method,[40] are summarized in Table 3. The lowest total strain energy corresponded to an isomer with two alcoholato groups in axial positions (model 2 in Chart 1), which is different from that found in the crystal structure of $Na[Cr^{V}O(ehba)_2]$ (two carboxylato groups in axial positions, model 1 in Chart 1).[18] The energetic preference for model 2 was confirmed in the MM calculations with no angle constraints on the Cr center, which produced a refined model very similar in energy (31.5 kJ mol^{-1}) and structure to model 2.[37] The results of this unrestrained calculation were used in MS XAFS modeling for $[Cr^{V}O(ehba)_2]^{-}$ and $[Cr^{IV}O(ehbaH)_2]^{0}$ complexes (see below). The isomer with one alcoholato group and one carboxylato group in axial positions (model 3 in Chart 1) was the least energetically favored one, as determined by MM calculations (Table 3). A comparison of the components of total strain energy for the three isomers (Table 3) showed the greatest difference was in the torsional deformation (only a very small component of the total energy) and the nonbonded interaction energy. The lowest strain energy level for model 2 is probably due to the largest distance between the most sterically demanding groups: the oxo group and the alkyl residues.[37] The increase in total strain energy correlated well with the increase in the angle between the two Cr−ligand planes (Table 3); similar correlations were observed in MM calculations for other Cr(V)−2-hydroxy-carboxylato complexes.[37] The small difference in strain energy between the isomers (∼4 kJ mol^{-1}, Table 3) compared to the total solvation energy of the ions in protic solvents (∼100 kJ mol^{-1})[1] is consistent with the existence of an equilibrium between at least two geometric isomers of $[Cr^{V}O(ehba)_2]^{-}$ in aqueous solutions.[42]

MS XAFS Fitting for Solid $Na[Cr^{V}O(ehba)_2]$. The results of MS XAFS fits of unknown structures may be affected by subjective choice of initial models and fitting parameters.[31] Therefore, a detailed study of the influence of these factors on the outcome of MS XAFS modeling was performed using a substance with known crystal structure, $Na[Cr^{V}O(ehba)_2]$.[18] Variation of the fitting conditions (Table S5, Supporting Information) led to changes in the R values,

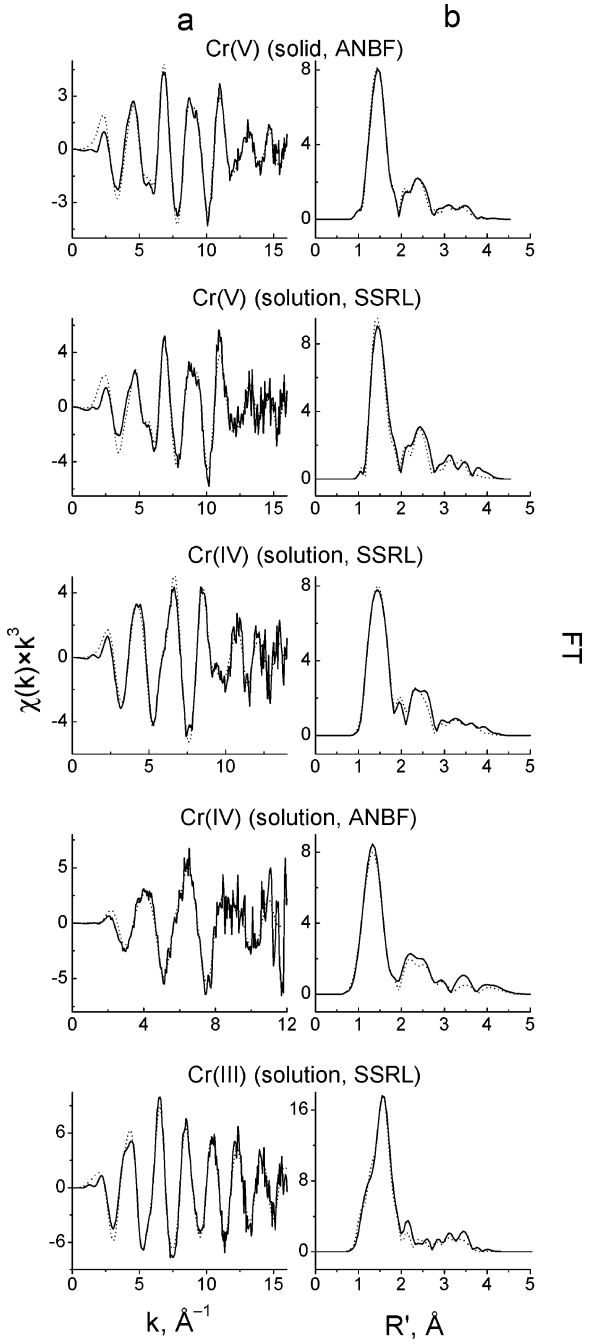

Figure 3. Experimental (solid lines) and calculated (dashed lines) XAFS (a) or FT XAFS (b) of the Cr(V/IV/III)−ehba complexes. For FT XAFS, both experimental and calculated spectra are windowed; applied window functions are shown in Figure S4, Supporting Information. The initial structures, used in the calculations, correspond to model 2 (for Cr(V) or Cr(IV)) or to model 4 (for Cr(III)) in Chart 1.

but did not affect, within experimental error,[31] the optimized values of Cr−O bond lengths and of the fitting parameters E_0, S_0^2, and σ_i^2 (the values of the parameters and the experimental errors are given in Table 2). All of the applied models were overdetermined ($N_i/p > 1$, Table S5); thus, the optimization results were valid for comparison of different models to determine the best fit to the data.[35] Experimental and calculated XAFS and FT XAFS spectra for the best fit (corresponding to row 2 in Table S5) are shown in Figure 3, and the corresponding FT window function is shown in Figure S4 (Supporting Information).

The ability of MS XAFS fittings to distinguish between geometric isomers of $Na[Cr^{V}O(ehba)_2]$ was tested. Three independent structures of $[Cr^{V}O(ehba)_2]^-$ were used to initialize the MS XAFS calculations: (i) the crystal structure of the Na^+ salt (corresponding to model 1 in Chart 1),[18] (ii) the energy-minimized structure, obtained from MM calculations,[37] and (iii) the structure generated by HyperChem software (the latter two structures corresponded to model 2 in Chart 1). Optimizations started from these models led to nonequivalent three-dimensional structures (the initial and optimized values of bond lengths and angles are listed in Table S6, Supporting Information), but the *R* values were close for all models (rows 1 and 3 or 2, 4, and 5 in Table S3). Restraining bond angles between the ligands close to those of the initial models[18,37] (±5°) led to significant deterioration of the fits ($R = 16\%$ vs 11%; rows 1 and 2 or 3 and 4 in Table S5). When no such restraints were applied, the optimized values of bond angles between the oxo ligand and the ehba ligands were model-dependent and significantly different from the initial values, while the values of bond angles between and within the ehba ligands did not change significantly during the optimizations (Table S6). Thus, the best fits obtained from MS XAFS calculations, using different starting models, did not lead to a unique three-dimensional structure; this is in agreement with the results obtained for the Cr(V)−quinato complex.[25] The calculations also did not show a significant preference toward one of the two geometric isomers (model 1 or 2 in Chart 1). However, the optimized values of the Cr−O bond lengths and bonding parameters within the ehba chelates did not depend on the initial models and were in excellent agreement with those found by X-ray crystallography (Table 2).[18] Identical values of metal−ligand bond lengths and Debye−Waller factors, within experimental error, were determined for the spectra of solid $Na[Cr^{V}O(ehba)_2]$, collected at either 10 or 293 K (Tables 2 and S6). Excluding Et groups of ehba ligands from the calculations did not lead to significant changes in the *R* values (rows 9 and 10 vs row 1 in Table S5), but further limiting the model by excluding the carboxylato O atoms caused significant deterioration of the fit (row 11 vs row 1 in Table S5). Further information on other changes to the models and the choice of final models for fitting the solution XAFS are detailed in the Supporting Information.

The ability of MS XAFS modeling to distinguish between the carboxylato and alcoholato donors in $[Cr^{V}O(ehba)_2]^-$ has been tested. This is particularly important since the difference in the lengths of the corresponding Cr−O bonds (~0.1 Å)[18] is on the resolution limit of SS XAFS calculations.[25,31] Restraining the Cr−O bond lengths for the carboxylato and alcoholato donors to be approximately equal (1.85 ± 0.05 Å) for model 1 (Chart 1; bond angles between the ligands were restrained) led to a significant deterioration of the fit ($R = 19\%$ vs 16%). When the bond length restraints were released, the Cr−O bond lengths returned to their correct values, and the *R* value returned to 16%. Deterioration of the fit (20% vs 16%) was also caused by restraining the Cr−O bonds in the "reversed order" (1.80 ± 0.05 Å for the carboxylato donors and 1.90 ± 0.05 Å for the alcoholato donors). However, in this case release of the bond length restraints did not improve the *R* value, and the right values of the bond lengths were not achieved. Thus, unlike for the SS XAFS, the MS XAFS fitting clearly distinguishes between the carboxylato and alcoholato donors in $[Cr^{V}O(ehba)_2]^-$. This feature is in agreement with the significant MS contributions of the carboxylato groups due to a nearly linear arrangement of the Cr−O−O vector (Table S7), irrespective of the model.

MS XAFS Modeling for the Solutions of Cr(V/IV/III)−ehba Complexes. Application of the MS models, based on the results of SS XAFS calculations, gave good fits for all three oxidation states of Cr. Experimental and calculated XAFS and FT XAFS spectra are shown in Figure 3 (the applied window functions are shown in Figure S4); optimized values of Cr−O bond lengths and the fitting parameters, as well as the *R* values, are listed in Table 2, and initial and optimized values of bond lengths and angles for different models are listed in Tables S8−S10, Supporting Information.

The results of MS XAFS modeling for the solution of $[Cr^{V}O(ehba)_2]^-$ (Table S8) are similar to those for the solid $Na[Cr^{V}O(ehba)_2]$ (Table S6): (i) calculations that started from three independent models led to different three-dimensional structures with close *R* values of the fits; the main differences in the optimized structures were the values of bond angles between the oxo ligand and the ehba ligands; (ii) restraining the bond angles between the ligands deteriorated the fits; (iii) optimized Cr−O bond lengths and σ_i^2 values were model-independent. Higher *R* values were obtained for the fit of the XAFS spectrum of the solution sample compared to that of the solid (Table 2), probably due to the increased noise in the solution XAFS compared to that of the solid (Figure 3).

For the data from solutions of $[Cr^{IV}O(ehbaH)_2]^0$ (Table S9), four independent models were used to initialize the MS XAFS calculations (for the data collected at the SSRL or ANBF): (i) the crystal structure of $Na[Cr^{V}O(ehba)_2]$,[18] (ii) the crystal structure of $NH_4[V^{IV}(ehba)(ehbaH)]$,[36] (iii) the energy-optimized MM structure of $Na[Cr^{V}O(ehba)_2]$,[37] and (iv) the structure of $[Cr^{IV}O(ehbaH)_2]^0$, generated by HyperChem software.[38] Geometries of the initial structures corresponded either to model 1 (i−ii) or to model 2 (iii−iv) in Chart 1. All four models led to identical (within experimental error) optimized Cr−O bond lengths and σ_i^2 values (Tables 2 and S9). Some deterioration of the fit ($R = 13.6\%$) was observed for the calculation that started from the structure of the V(IV)−ehba complex, while the other three models led to close *R* values (11.9−12.5%, Table S9). The optimized Cr−O bond lengths, 1.56 Å (oxo), 1.90 Å (carboxylato), and 2.00 Å (protonated alcoholato), were the same for the data collected at the SSRL or at the ANBF, and corresponded, within experimental error, to analogous bond lengths in the crystal structures of $[Cr^{V}O(ehba)_2]^-$ and $[V^{IV}O(ehba)(ehbaH)]^-$.[18,36] Restraining the Cr−O bond lengths for the carboxylato and alcoholato donors to be approximately equal (1.95 ± 0.05 Å) led to significant deterioration of the fit ($R = 20\%$ vs 12% for the SSRL data). Release of the bond length restraints led to the restoration of the initial values

(1.90 Å for the carboxylato donors and 2.00 Å for the alcoholato donors). Thus, as in the case of $[Cr^{V}O(ehba)_2]^-$, application of MS XAFS fitting allowed a clear distinction between the two types of O donors within the ehba ligand, which was not possible using the SS XAFS fits.[25,31] As for the Cr(V) complex, the main differences in the optimized structures of the Cr(IV) complex that were obtained with the various starting models were in the bond angles between the oxo ligand and the ehba ligands (Table S9).

Four independent models were used to initialize the MS XAFS calculations for the solution of $[Cr^{III}O(ehbaH)_2(OH_2)_2]^+$ (Table S10), corresponding to different geometric isomers, including those with the *cis* or *trans* positions of H_2O ligands (models 4−7 in Chart 1; four of the five possible isomers were considered); all models were generated by HyperChem software.[38] Calculations started from models 4−7 yielded nonequivalent three-dimensional structures; however, the *R* values were close for all models (16.7−17.0%), and the optimized Cr−O bond lengths and σ_i^2 values were the same, within experimental error (Tables 2 and S10). The optimized Cr−O bond lengths, 1.97 Å (H_2O), 1.90 Å (carboxylato), and 1.98 Å (protonated alcoholato), were in excellent agreement with the corresponding bond lengths in $[Cr^{III}(OH_2)_6]^{3+}$ (1.97 Å, determined by MS XAFS analysis),[49] and in a crystallographically characterized Cr(III)−tartrato complex (1.91 Å for the carboxylato donor and 1.98 Å for the protonated alcoholato donor).[50] However, the weaker MS contributions evident in the FT of the XAFS compared to those of Cr(V) and Cr(IV) makes the MS differentiation of these different bond lengths less certain.

Discussion

Influence of Sample Photodamage. Like Fe(III) heme proteins,[31] complexes of Cr in high oxidation states are susceptible to photoreduction during the X-ray irradiation, even at liquid He temperatures (10 K). Data of UV−vis spectroscopy (Figure 1) suggest that at least 90% of total Cr in the bulk solution samples of Cr(V/IV/III)−ehba complexes is retained in its initial oxidation state after the irradiation by the focused X-ray beam at the SSRL. The degree of photodamage cannot be assessed quantitatively from the UV−vis spectroscopy data, as thawing and warming of the samples leads to two opposite effects: (i) additional reduction of Cr(V/IV) species by trapped electrons and (ii) dilution of photodamaged molecules from the irradiated spots by the bulk of the sample. Monitoring of the XANES (Figure S1) allowed the rejection of the affected scans, so that the data quality is not compromised.[31] However, this method also does not allow a simple estimation of the degree of photodamage, as evident from the much smaller changes in the pre-edge absorbance, compared with those at the edge (Figure S1a,b). One possible reason for this is the formation of thermodynamically unstable intermediates (e.g., $[Cr^{IV}O(ehba)_2]^{2-}$ in the reduction of $[Cr^{V}O(ehba)_2]^-$).

The results of XAS data analyses for $[Cr^{V}O(ehba)_2]^-$ in solution (most affected by photodamage, Figure S1) and for the solid $Na[Cr^{V}O(ehba)_2]$ (negligible photodamage) were the same, within experimental error, and corresponded to the crystal structure of the Cr(V) complex (Table 2, Figures 2 and 3). The same results, within experimental error (Table 2, Figure S2), were obtained for the solutions of $[Cr^{IV}O(ehbaH)_2]^0$ when the spectra were collected at the SSRL (significant photodamage, Figure S1b) or at the ANBF (negligible photodamage, Figure S1d). Thus, the results of XAS data analysis (Table 2) were not significantly affected by the sample photodamage, if appropriate precautions were taken to reject affected data.

Solid-State and Solution Structures of $[Cr^{V}O(ehba)_2]^-$. Application of MS analyses to the XAFS spectra of $Na[Cr^{V}O(ehba)_2]$ (as well as $[Cr^{IV}O(ehbaH)_2]^0$) leads to a definitive distinction between the carboxylato and alcoholato donors, which is not possible using the SS XAFS calculations. According to the crystal structure,[18] solid $Na[Cr^{V}O(ehba)_2]$ possesses a distorted trigonal-bipyramidal geometry with carboxylato ligands in axial positions, corresponding to model 1 in Chart 1. Multiple-scattering XAFS fittings for the powder sample of $Na[Cr^{V}O(ehba)_2]$, as well as for its frozen aqueous solution, reproduce well the Cr−O bond lengths and the bond angles between the ehba ligands, but do not reproduce the bond angles between the oxo ligand and the ehba ligands, found in the crystal structure (Tables S6 and S8). There are two independent sites with slightly different conformations in the crystal structure of this complex,[18] but the bond lengths and angles in the first coordination sphere are the same within the errors of XAFS determinations. However, EPR studies showed that both isomers were present on dissolution of the microcrystals. The presence of two geometric isomers of $[Cr^{V}O(ehba)_2]^-$ on dissolution is manifested by the splitting of outer signals due to ^{53}Cr hyperfine coupling, since interconversions of such isomers (Berry twists) are slow on the EPR time scale and occur over a matter of minutes.[1,51] If only one isomer were present in the sample, only one peak would be observed on dissolution. The virtually identical g_{iso} values in the EPR spectrum show that the donor (Cr−O) bond lengths in the two geometric isomers are very close, whereas the significantly different A_{iso} values demonstrate that the bond angles must be significantly different in the two geometric isomers. It is not clear whether the MS fitting could come to a unique solution for the O−Cr−O bond angles in the absence of isomers because of the weaker MS contributions involving these angles as compared to those in the Cr−carboxylato group (Table S7). As outlined earlier, the latter contributions do enable MS to distinguish between the Cr−OCOR and Cr−OR/Cr−OHR groups. The MS XAFS results are also consistent with the molecular mechanics calculations that showed a small energy difference among potential isomers (Table 3). The similarities in the solution and solid-state XANES and XAFS spectra of $[Cr^{V}O(ehba)_2]^-$ (Figures 2 and

(49) Sakane, H.; Muños-Páez, A.; Díaz-Moreno, S.; Martínez, J. M.; Pappalardo, R. R.; Sánchez, M. E. *J. Am. Chem. Soc.* **1998**, *120*, 10397−10401.
(50) Ortega, R. B.; Tapscott, R. E.; Campana, C. F. *Inorg. Chem.* **1982**, *21*, 2517−2519.
(51) (a) Branca, M.; Micera, G.; Segre, U.; Dessì, A. *Inorg. Chem.* **1992**, *31*, 2404−2408. (b) Branca, M.; Dessì, A.; Micera, G.; Sanna, D. *Inorg. Chem.* **1993**, *32*, 578−581.

3) confirm the deduction, made on the basis of EPR spectroscopy, that the five-coordinate structure of the Cr(V) complex is retained in solutions[23] and disprove the hypothesis[52] that, in the presence of excess ligand, a third ligand molecule binds to $[Cr^{V}O(ehba)_2]^-$ in a monodentate fashion, leading to a six-coordinate octahedral structure.

Solution Structure of $[Cr^{IV}O(ehbaH)_2]_0$. Detailed MS XAFS studies confirmed preliminary results[26] on the general description of the solution structure of the Cr(IV) complex, but did not confirm the previously found significant differences in the Cr−O(alcohol) bond lengths between the two ehba ligands.[26] The latter result was probably an artifact of the higher noise level and smaller k range in the XAFS spectrum in the preliminary work[26] ($k_{max} = 11$ compared to 14 in this work). The alternative structure of the complex, $[Cr^{IV}(ehbaH)_2(OH)_2]^0$, proposed by Gould and co-workers,[22] is inconsistent with the results of SS XAFS calculations (Table S4) and with a significant difference in FT XAFS amplitude between the Cr(IV)−ehba complex and the six-coordinate Cr(III)−ehba species (Figure 2b). No structural data on the Cr(IV) complexes with O donor ligands, similar to $[Cr^{IV}O(ehbaH)_2]^0$, are available for comparison. The lengths of the Cr═O and Cr−O(alcohol) bonds in this complex (Table 2) are close to those for the Cr═O (1.57 Å) and Cr−N (2.03 Å) bonds in a crystallographically characterized Cr(IV)−oxo−porphyrinato complex.[53]

The main difference in the structures of Cr(IV)− and Cr(V)−ehba complexes is the protonation of alcoholato ligands in the former complex, which makes the Cr(IV)−ehbaH complex more labile in solutions compared with its Cr(V) counterpart. This feature explains the different chemical properties of the Cr(IV) complex, compared with those of the Cr(V) complex, including (i) the pH dependency of UV−vis spectra due to the formation of $[Cr^{IV}O(ehba)(ehbaH)]^-$,[13] (ii) the easy loss of one ehba ligand with the formation of monochelated Cr(IV)−ehba complexes,[20,21] (iii) the stronger oxidizing power of the Cr(IV) complex,[23] and (iv) the higher rates of disproportionation compared to the Cr(V) complex.[20,21] The lower ability of Cr(IV), compared with Cr(V), to deprotonate alcoholato ligands also explains why Cr(IV), unlike Cr(V), is not stabilized by biologically important 1,2-diolato ligands, such as carbohydrates and glycoproteins.[4,5,21] In neutral aqueous solutions, Cr(IV) is less likely than Cr(V) to cause oxidative cleavage of DNA and other biomolecules.[7,12−14]

Solution Structure of $[Cr^{III}(ehbaH)_2(OH_2)_2]^+$ and the Mechanism of Electron Transfer in the Cr(V/IV/III)−ehba Redox Series. The results of SS and MS XAFS fitting for a Cr(III) product, formed in the fast reaction of $[Cr^{V}O(ehba)_2]^-$ with excess Fe(II) at pH 3.5, are in agreement with the structure assigned from the UV−vis spectroscopic and ion-exchange studies.[30] No strong preference was determined for one of the possible geometric isomers over the others (models 4−7 in Chart 1) from the XAFS calculations. The reaction of $[Cr^{V}O(ehba)_2]^-$ with Fe(II) is known to pass through Cr(IV)−ehba intermediates, which are rapidly reduced by excess Fe(II).[30] The XAFS spectroscopic studies of Cr(V/IV/III)−ehba complexes confirmed the results of electrochemical studies, showing that major structural transformation occurs in the Cr(IV)/Cr(III) redox couple, not in the Cr(V)/Cr(IV) redox couple (Scheme 1). [23]

Scheme 1. Proposed Structures and Mechanism of Electron Transfer in Cr(V/IV/III)−ehba Complexes

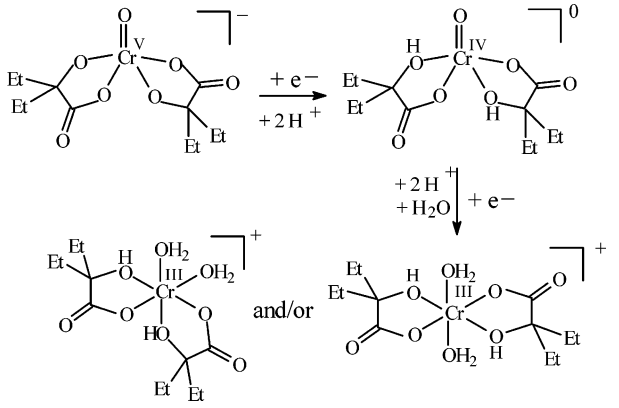

Bond Valence Sum Analysis. A correlation between the bond lengths and Cr oxidation states in the Cr complexes with O donors has been recently established.[54] Determination of Cr−O bond lengths in $[Cr^{IV}O(ehbaH)_2]^0$ and in $[Cr^{III}(ehbaH)_2(OH_2)_2]^+$ by MS XAFS analysis, together with the crystallographic and XAFS data for $[Cr^{V}O(ehba)_2]^-$ (Table 2), allows a check of the applicability of this correlation to the Cr(V/IV/III)−ehba redox series. The oxidation states (z), estimated as

$$z = \sum(\exp((R_0 - R)/b)) \qquad (1)$$

where R is a Cr−O bond length, $R_0 = 1.724$ Å is an average bond length of unit valence, and $b = 0.37$ is a correlation coefficient,[51] were 4.42, 3.80, and 3.26 for the Cr(V)−, Cr(IV)−, and Cr(III)−ehba complexes, respectively. Thus, application of the valence bond sum analysis to the Cr−ehba complexes, with the use of bond lengths determined from XAFS data analysis, allows a prediction of the Cr oxidation states in these complexes (error ≤12%).

Conclusions. Aqueous solution structures of the Cr(V/IV/III)−ehba complexes (Scheme 1) have been determined from the SS and MS fitting of their XAFS spectra in frozen solutions (10 K). These results solve the controversies over the solution structure of the Cr(V)−ehba complex, the structure of the Cr(IV)−ehba complex, and the mechanisms of electron transfer in the Cr(V/IV/III)−ehba series.[22,23]

Acknowledgment. Financial support of this work was provided by an Australian Research Council (ARC) grant (to P.A.L.) and an ARC grant for the fluorescence detector at the ANBF. This work was supported by the Access to Major Facilities Program funded by the Department of Industry, Science and Resources and managed by the

(52) Fanchiang, Y.-T.; Bose, R. N.; Gelerinter, E.; Gould, E. S. *Inorg. Chem.* **1985**, *24*, 4679−4684.
(53) Groves, J. T.; Kruper, J. W. J.; Haushalter, R. C.; Butler, W. M. *Inorg. Chem.* **1982**, *21*, 1363−1368.
(54) Wood, R. M.; Abboud, K. A.; Palenik, R. C.; Palenik, G. J. *Inorg. Chem.* **2000**, *39*, 2065−2068.

Australian Nuclear Science and Technology Organisation. X-ray absorption spectroscopy was performed partially at the ANBF with support from the Australian Synchrotron Research Program, which is funded by the Commonwealth of Australia under the Major National Research Facilities program, and partially at the SSRL, which is operated by the Office of Basic Energy Sciences, U.S. Department of Energy. The SSRL Biotechnology Program is supported by the National Institutes of Health, National Center for Research Resources, Biomedical Technology Program, and the Office of Biological and Environmental Research, U.S. Department of Energy. We thank Dr. James Hester (ANBF) and Dr. Colin Weeks (University of Sydney) for assistance at the ANBF and Drs. Britt Hedman, Paola de Cecco, Matthew Latimer, and Samuil Belopolsky for assistance at the SSRL.

Supporting Information Available: Further information on the results of different MS models, figures showing the changes in XANES spectra due to photodamage, comparison of X-ray absorption spectra of $[Cr^{IV}O(ehbaH)_2]^0$ solutions, collected at the SSRL or at the ANBF, comparison of XANES spectra of $[Cr^{IV}O(ehbaH)_2]^0$ and CrO_2, and window functions applied to MS XAFS calculations and tables showing the details of SS and MS XAFS and MM calculations. This material is available free of charge via the Internet at http://pubs.acs.org.

IC030239R